

Article

Synthesis of Integrated Material with Activation and Oxidation Functions by Mechanical Milling of Activated Carbon and Persulfate for Enhanced Tetracycline Degradation over Non-Radical Mechanism

Peng Tan, Nuo Meng, Xuxin Cao, Xiguo Zhang, Yuanyuan Huang, Tielong Li * and Wei Wang *

MOE Key Laboratory of Pollution Processes and Environmental Criteria, Tianjin Key Laboratory of Environmental Technology for Complex Trans-Media Pollution, College of Environmental Science and Engineering, Nankai University, Tianjin 300350, China; t15215077520@163.com (P.T.); 2120220760@mail.nankai.edu.cn (N.M.); 2120220822@mail.nankai.edu.cn (X.C.); zhangxiguohu@163.com (X.Z.); yyhdyx068@163.com (Y.H.)

* Correspondence: litielong@nankai.edu.cn (T.L.); nkawangwei@126.com (W.W.); Tel.: +86-022-23501117 (T.L. & W.W.)

Abstract: As an alternative to the traditional advanced oxidation process of adding potassium persulfate (PS) and its activator to the solution separately, in this study, M(AC-PS), an integrated activator and catalyst, was synthesized by vacuum ball milling of PS and activated carbon (AC) to improve the PS's utilization efficiency. The joint mechanical milling caused a change in the preferentially exposed crystal surface of the PS and the generation of more π - π^* structures on the AC, leading to successful and stable connection of the PS onto the surface of the AC. Within 40 min, the M(AC-PS) achieved a degradation rate of 97.3% for tetracycline (TC, 20 mg/L), while the mixed system where AC and PS were separately ball milled achieved only a 53.1% removal of TC. Reactive oxygen species and electrochemical tests showed that M(AC-PS) mainly oxidized TC through non-free radical mechanisms. In M(AC-PS), AC provided oxygen-containing functional groups (e.g., C=O) to activate the PS and electron holes as an electron transfer medium, generating $^1\text{O}_2$ and promoting electron donation from the TC to enhance the oxidation of the TC. Almost no catalytic components were detected in the solution, indicating that the obtained solid composite material avoids the limitations of solid-liquid interface contact and mass transfer, and then improves the efficiency of activation and catalysis. This study presents a simple and feasible method for obtaining efficient and convenient material for the advanced oxidation treatment of wastewater.

Keywords: activated carbon; potassium persulfate; ball milling; tetracycline; non-radical mechanism



Citation: Tan, P.; Meng, N.; Cao, X.; Zhang, X.; Huang, Y.; Li, T.; Wang, W. Synthesis of Integrated Material with Activation and Oxidation Functions by Mechanical Milling of Activated Carbon and Persulfate for Enhanced Tetracycline Degradation over Non-Radical Mechanism. *Processes* **2024**, *12*, 672. <https://doi.org/10.3390/pr12040672>

Academic Editor: Juan García Rodríguez

Received: 6 March 2024

Revised: 25 March 2024

Accepted: 26 March 2024

Published: 27 March 2024



Copyright: © 2024 by the authors. Licensee MDPI, Basel, Switzerland. This article is an open access article distributed under the terms and conditions of the Creative Commons Attribution (CC BY) license (<https://creativecommons.org/licenses/by/4.0/>).

1. Introduction

Antibiotics have been routinely utilized in various fields, including human medical treatment and animal husbandry. However, their excessive use and persistence in the environment have led to their emergence as a new type of pollutant [1]. China is the largest consumer of antibiotics globally, with a significant portion of antibiotics being excreted and released into domestic sewage while still retaining their biochemical activity [2]. As a result, these antibiotics contaminate surface water, groundwater, and sediment, leading to severe water pollution [3]. Moreover, the overuse of antibiotics can lead to the generation of antibiotic resistance genes, posing a major threat for human health [4]. Tetracycline (TC) is one of the antibiotics which is most extensively used worldwide due to its stable chemical structure and antibacterial properties [5]. As a broad-spectrum antibiotic, it is widely used in the medical treatment and prevention of human and animal diseases because of its low price and effective bactericidal performance. Meanwhile, TC is also widely applied in aquaculture, animal husbandry, and agricultural production as a growth promoter [6]. The

excessive use and incomplete treatment of TC will cause serious harm to human health and the environment [7]. Consequently, there is an urgent need to identify efficient and suitable approaches for the degradation of TC [8].

Recently, various new materials have emerged that can be used in the physical and chemical techniques to treat drugs and dyes, including adsorption, coagulation, filtration, and degradation [9–13]. Compared with other methods, chemical catalysis is considered an effective environmental pollution control and energy conversion technology which has the advantages of high catalytic efficiency, low energy consumption, and good applicability, and, therefore, has a wide application prospect. In recent decades, advanced oxidation processes (AOPs) have been proposed as effective catalytic techniques to treat organic pollutants in wastewater [14]. AOPs utilize strong oxidants to generate highly reactive species that can directly oxidize and convert organic pollutants into simpler, biodegradable compounds. Among the different AOPs, persulfate (PS)-based AOPs have gathered significant interest due to the production of abundant sulfate radicals ($\text{SO}_4^{\cdot-}$) for oxidation reactions [15]. Compared with traditional Fenton reactions producing hydroxyl radicals ($\cdot\text{HO}$), PS-based AOPs have the characteristics of excellent selectivity, strong oxidation performance, wide application range of pH, and no secondary pollution [16]. Sulfate radicals exhibit a longer half-life and higher oxidation efficiency, making them highly promising for various applications [17]. To ensure the oxidation ability, PS needs to be activated to generate $\text{SO}_4^{\cdot-}$. Various methods, including ultrasound, heating, light, transition metals, and so on, have been employed to activate persulfate [18]. However, these activation methods have the drawbacks of high consumption and low application performance.

Due to the problem of metal ion leaching, some non-metallic carbon materials, such as activated carbon (AC), carbon nanotubes (CNT), biochar (BC), and graphite, have become alternative solutions for PS activation [18]. According to the report, the FeS@BC/PS system can achieve a 90% degradation rate for 200 mg/L tetracycline (TC). BC can inhibit the aggregation of catalyst, ensure the effective utilization of FeS, and serve as the adsorption substrate and electron shuttle, promoting the electron transfer between pollutants and oxidants [19]. Guan et al. found that the CNT/PDS system showed good activation performance and stability for the degradation of sulfamethoxazole through non-radical mechanisms even at lower pH levels [20]. Oh et al. demonstrated that the $\text{CuFe}_2\text{O}_4/\text{AC}$ system exhibits excellent activation and adsorption properties as well as recyclability, with AC being used as a catalyst for PMS activation and as a renewable adsorbent [21]. Among these catalysts, AC stands out as the most extensively utilized carbon material for PS-based AOPs. AC is easy to obtain and possesses a high specific surface area, is abundantly porous, and has active functional groups, making it more cost-effective compared to other carbon materials [22]. AC has four main active sites involved in PS activation, including sp^2 hybrid carbon at defective edges, oxygen-containing functional groups, delocalized π electrons, and surface defects [16,23]. These active sites can activate PS to produce strong oxidative free radicals, such as $\text{SO}_4^{\cdot-}$ and/or HO^{\cdot} [24]. However, in existing studies, AC and PS are added to the solution separately, and the dissolved PS and pollutants compete for adsorption sites on the surface of the AC (which has strong adsorption capacity), which is unfavorable for PS activation and pollutants' degradation. To our knowledge, there have been no reports about a solid composite of PS and AC to directly activate PS for catalytic degradation of pollutants. Typically, PS in the solution needs to be adsorbed on the solid AC first, and then the activation products oxidize the pollutants.

The preparation of composite materials usually uses chemical methods, especially in the synthesis of composite carbon materials, which require a high temperature or a significant amount of chemical reagent for thermal or hydrothermal synthesis. Compared to physical methods [25], these chemical processes tend to consume more energy and materials. Ball milling is a powerful physical non-equilibrium processing method that can mechanically reduce the grain size of solids, generating ultrafine particles [26]. During the ball milling process, local micro regions with high temperature and high pressure are formed, and the mechanical effects such as shearing, compression, and grinding can

provide the energy required for chemical reactions. This is an efficient and economical material composite technology [27] and has been employed to synthesize some carbon-based nanocomposites, aiming to improve the properties of materials in the following ways: (i) the macro-scale materials can be transformed into nano-scale particles with higher surface activity through mechanical ball milling; (ii) the high-energy effect in the grinding process can produce a series of functional groups on the surface of the material to improve the reactivity and electron transfer capacity; and (iii) two or more materials can be mixed to form a solid to change the way the reaction proceeds [28,29]. Nowadays, most carbon-based materials prepared by mechanical methods are composited with transition metal to suppress the leakage of metal ions, and these obtained composite materials are used to investigate the ability of metal and carbon materials to jointly activate liquid phase PS. The preparation of non-metallic composite catalysts by direct ball milling of solid AC and PS has not been reported yet. Whether AC can effectively activate PS in composite is still unknown.

The commonly used PS activation methods mainly involve reactions in the liquid-phase system or across the solid–liquid interface. Additionally, in advanced oxidation processes involving PS, there are still limitations such as narrow pH application range, easy dissolution or limited interfacial mass transfer of catalyst, low synthesis yield, and high costs. Herein, a direct composite material of non-metal carbon catalyst and solid oxidant was innovatively obtained through a high-yield and low energy consumption approach. This is different from the traditional process of adding PS to the solution. In this study, a solid composite material composed of AC and PS (M(AC-PS)) is successfully synthesized using a simple physical ball milling method, forming a novel AOPs material that combines catalytic and oxidation functions. The interaction between AC and PS occurs directly in the solid catalyst, avoiding the limitation of interfacial mass transfer, ensuring the full reaction of PS, and providing an integrated utilization for activator and oxidant. The goals of the present research are to verify the activation ability of the AC on the PS bound to it, investigate the TC degradation performance of M(AC-PS) obtained under different AC and PS dosage ratios, analyze the influence of reaction conditions (pollutant concentration, initial pH, inorganic anion, and natural organic matter) on catalytic oxidation performance, evaluate the stability of composite materials, and reveal the activation mechanism of solid composite system.

2. Experimental Procedure

2.1. Reagents and Materials

Activated carbon (AC) was purchased from Sigma-Aldrich (Shanghai, China). Tetracycline hydrochloride (TC) and potassium persulfate ($K_2S_2O_8$, PS) were obtained from Titan Technology (Shanghai, China). Sodium nitrate ($NaNO_3$), sodium bicarbonate ($NaHCO_3$), sodium chloride ($NaCl$), sodium sulfate (Na_2SO_4), humic acid (HA), potassium iodide (KI), and L-histidine were purchased from Aladdin Technology (Shanghai, China). Spin trapping reagents, including 5,5-dimethyl-1-pyrrolin-n-oxide (DMPO) and 2,2,6,6-tetramethylpiperidine (TEMP), were obtained from Huaxun Medical Technology (Tianjin, China). Distilled water was used to prepare the chemical solutions for the experiments. All chemicals used were of analytical grade, and no additional purification was required.

2.2. Preparation of Ball Milled Carbon Materials

In the ball milling preparation, 1 g of activated carbon (AC) and different dosages of PS were used to obtain M(AC-PS) with different AC and PS mass ratios (1:1, 1:2.5, 1:5, 1:8, and 1:10). AC and PS mixture was added to a zirconia ball mill (Shanghai Jingxin Industrial Development Co., Ltd., Shanghai, China), and then agate balls with diameters of 3, 6, and 15 mm were used as the grinding medium in the mass ratio of 3:5:2 (100 g total). After blowing with nitrogen for 20 min, the ball mill ran at a rotational speed of 300 rpm. The composite materials were ground for 12 h. The rotation direction of ball mill changed every 3 h, with a 5 min rest period between rotations. Finally, the ball milled composite carbon

material was collected and stored in a dry centrifuge tube. The obtained composite carbon material, with an AC/PS ratio of 1:1, 1:2.5, 1:5, 1:8, and 1:10, was named as M(AC-PS)₁, M(AC-PS)₂, M(AC-PS)₃, M(AC-PS)₄, and M(AC-PS)₅, respectively. Additionally, AC and PS were separately ball milled using the aforementioned method, and the resulting samples were named as MAC and MPS.

2.3. Characterization Method

The crystallinity of PS, MPS, AC, MAC, and M(AC-PS) before and after the pollutant degradation reaction was determined by X-ray powder diffraction (XRD) (Rigaku Corporation, UlitmaIV, Tokyo, Japan). Fourier transform infrared spectroscopy (FTIR) was performed on the tensor 37 FTIR spectrometer (BRUKER, Mannheim, Germany) to determine functional groups in the above-mentioned substances. The morphology and size of MAC and M(AC-PS) were characterized by a JEM-2800 transmission electron microscopy (TEM) (JEOL, Tokyo, Japan) at 200 kV. X-ray photoelectron spectroscopy (XPS) (Thermal Science Laboratory 250Xi, Thermo, Waltham, MA, USA) and the multi-station Extended Automatic Rapid Surface Comparator (Micromeritics, ASAP 2460, Norcross, GA, USA) were used to determine the surface element composition, specific surface area, and pore size and distribution of sample. The electrochemical measurements, including cyclic voltammetry (CV), linear sweep voltammetry (LSV), and transient photocurrent (IT), were conducted with a CHI 760E electrochemical workstation (CH Instrument, Chenhua, Shanghai, China) in a standard three-electrode system using Ag/AgCl electrode as reference electrode and platinum plate as counter electrode. The MAC or M(AC-PS) working electrode was prepared by ultrasonically dispersing 5 mg of the material in a mixture of 0.4 mL Nafion, 0.1 mL of water, and 0.5 mL of ethanol, and then depositing two drops of the mixture onto a polished iron disc electrode (EIS). The electrolyte solution used was a 0.1 mol·L⁻¹ sodium chloride solution, which was not stirred or deoxygenated during the measurement process.

2.4. Degradation Experiments

All degradation experiments were conducted in 100 mL closed reaction bottles at a controlled temperature of 25 °C (±2 °C) on a shaker (Changzhou Danrui experimental equipment Co., Ltd., Changzhou, China) operating at 200 rpm for a duration of 40 min. The initial concentration of TC solution used is 20 mg/L. In the comparative experiments, PS (1 mM), MPS (1 mM), AC (0.1 g/L), MAC (0.1 g/L), mixture of AC and PS, mixture of MAC and MPS, and M(AC-PS) (AC = 0.1 g/L, PS = 1 mM) were added to the reaction systems, respectively. The initial pH (pH 3–11) of solution was adjusted using 0.1 M sodium hydroxide or hydrochloric acid. At regular intervals, 1 mL of the suspension was withdrawn using a syringe, followed by centrifugation and filtration through 0.22 µm filter for subsequent analysis.

2.5. Analytic Methods

The sample solution was measured by a high-performance liquid chromatograph (HPLC, Ultimate 3000, ThermoFisher, USA) equipped with C18 column (3 µm, φ3.0 × 100 mm) to calculate the removal rate of TC, and the PS concentration in solution was determined by potassium iodide spectrophotometry using an ultraviolet–visible spectrophotometer (UV-VIS) (Shanghai Yi electric Analytical Instrument Co., Ltd., Shanghai, China) [30]. The reactive oxidative species generated during the reaction were determined by electron paramagnetic spectrometer (EPR) (Bruker, Germany).

3. Results and Discussion

3.1. Characterization of Materials

Figure S1 shows the TEM images of AC and M(AC-PS) (AC:PS mass ratio = 1:2.5). The original AC appears as a layered structure. During the mixing and milling process, AC and PS undergo collision, friction, and compression, resulting in fracture, aggrega-

tion, and deformation [29]. It can be observed that the obtained composite material has undergone significant changes, exhibiting a block-like structure, while PS is attached to the AC. Energy-dispersive X-ray spectroscopy (EDS) mapping (Figure 1) reveals that the M(AC-PS) composite materials consist of C, O, and S elements, while O and S elements are uniformly distributed on the C substrate. All the distribution regions of the S and O elements overlap, as the O and S in the PS are directly connected. The EDS element analysis (Figure S2) also reflects that the main elements in the composite material are C, O, and S, with a mass ratio of S to O of 1:2, consistent with the mass ratio of S and O in PS. It can be seen that the PS has successfully combined with the AC, forming a uniformly distributed AC-PS composite material.

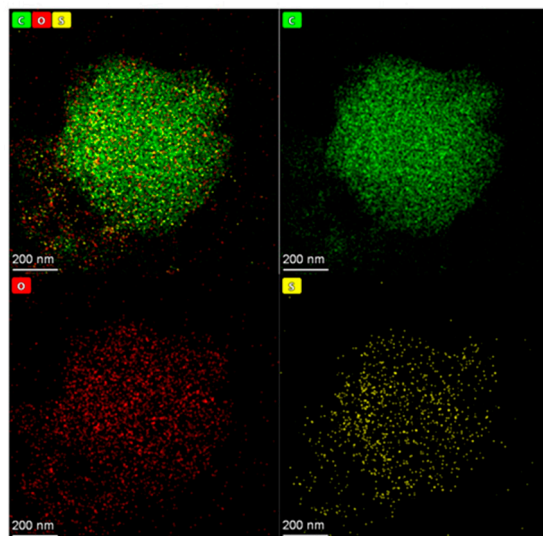


Figure 1. Energy-dispersive X-ray spectroscopy mapping of M(AC-PS).

N_2 adsorption–desorption isotherms were obtained to determine the specific surface area (BET) and pore size distribution of AC, MAC, and M(AC-PS) (Figure 2a,b), and the detailed parameters are summarized in Table 1. All carbon materials exhibit Type I adsorption isotherms with narrow hysteresis loops, indicating their sorption behavior at low relative pressures [31]. AC exhibits strong adsorption capacity, the adsorption capacity of MAC is lower than that of AC, while M(AC-PS) gradually loses its adsorption performance with the increase in PS dosage. The pore size distribution analyses reveal that AC and MAC have a large number of micropores and mesopores, forming a hierarchical pore structure. Mesopores are mainly distributed on the surface of M(AC-PS)₁, but the pores of M(AC-PS)_(2,3,4,5) are significantly reduced. Table 1 shows that the ball milling process leads to a decrease in the specific surface area (from 1503.55 to 668.57 m²/g), pore volume (from 1.068 to 0.438 cm³/g), and average pore size (from 2.63 to 0.63 nm) of the AC, indicating the pore collapse in AC caused by the high-energy impacts during ball milling [32]. After the addition of PS for mixed ball milling with AC, the specific surface area and pore volume of M(AC-PS) continue to decrease. This can be attributed to the binding of PS with AC, where the PS occupies a portion of the pores on the AC. However, the average pore size of M(AC-PS) increases with the increase in the PS dosage. This may be due to the oxidation property of PS, which enlarges the pore of the AC through oxidation during ball milling, resulting in an increased in the pore size of M(AC-PS) [33]. Wang et al. reported that a pore size of around 5 nm on carbon is most conducive to the diffusion and adsorption of TC. Mesopores exhibit better adsorption performance, with the optimal adsorption occurring at a pore size of 5.98 nm [34]. According to the surface structure analysis of various materials, AC has stronger adsorption capacity for TC than for MAC, and the ball milling process reduces the adsorption performance of AC. The adsorption capacity of obtained M(AC-PS) series materials significantly decreased.

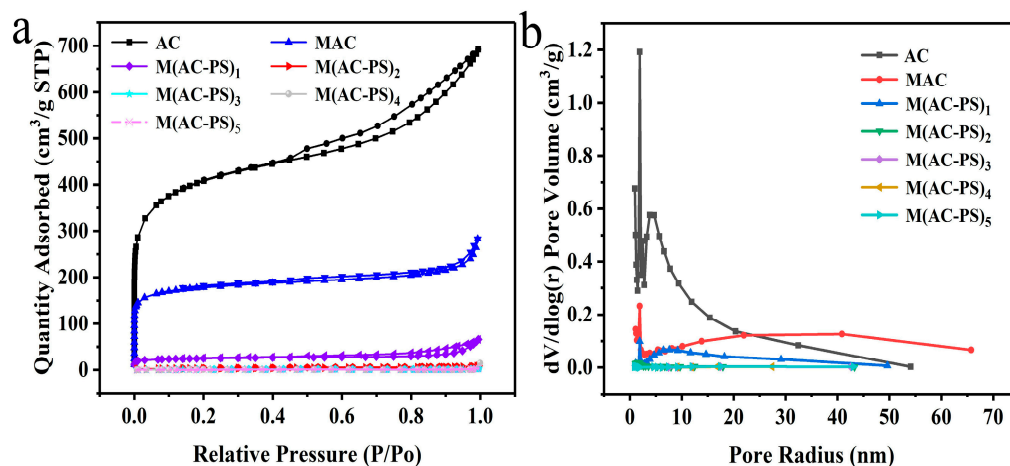


Figure 2. (a) N_2 adsorption/desorption isotherm and (b) Barrett–Joyner–Halenda aperture distribution of various materials.

Table 1. Surface structure analysis of M(AC-PS).

| | AC | MAC | M(AC-PS) ₁ | M(AC-PS) ₂ | M(AC-PS) ₃ | M(AC-PS) ₄ | M(AC-PS) ₅ |
|------------------------------|---------|--------|-----------------------|-----------------------|-----------------------|-----------------------|-----------------------|
| BET surface area (m^2/g) | 1503.55 | 668.57 | 92.26 | 10.94 | 3.91 | 2.58 | 3.48 |
| Pore volume (cm^3/g) | 1.068 | 0.438 | 0.100 | 0.013 | 0.004 | 0.015 | 0.004 |
| Average pore size (nm) | 2.63 | 0.63 | 5.61 | 2.29 | 21.04 | 18.96 | 3.91 |

As shown in the XRD patterns of Figure 3a, AC exhibits characteristic peaks at 23.3° and 44.2° , corresponding to amorphous carbon (002) and crystalline carbon (101), respectively. These results are consistent with previous reports [35]. By comparison, the crystallization degree of MAC improved after ball milling. In the spectrum of PS, there is a prominent peak corresponding to the (020) crystal plane of $K_2S_2O_8$ located at 27.6° . While, for MPS, more characteristic peaks can be observed at 18.2° , 24.2° , and 25.8° . These peaks can be assigned to the crystal planes (–110), (1–11), and (101) of $K_2S_2O_8$ (PDF#32-0846). It can be seen that more crystal planes of $K_2S_2O_8$ are exposed through the ball milling process. The XRD pattern of M(AC-PS) simultaneously contains the characteristic peaks of AC and PS. It is noteworthy that the diffraction peak at 24.2° corresponding to the (1–11) crystal plane of $K_2S_2O_8$ is significantly enhanced, indicating a change in the preferentially exposed crystal plane of composite material. It may be formed by the interleaving of the crystal faces of the AC and PS. This crystal plane may be more conducive to the link formation between AC and PS. Additionally, mixed ball milling may produce more lattice defects and smaller crystallite size, causing peak broadening of M(AC-PS). The crystal structure of M(AC-PS) after the reaction is similar to that of AC, indicating that the PS in the composite is consumed during the reaction process, and there are also active structures on the surface of the MAC that participate in the reaction.

The surface functional groups of various materials were characterized by FTIR spectroscopy (Figure 3b). The results show that the types of functional groups on PS and AC do not change significantly after milling. For M(AC-PS), the characteristic peaks of AC are at 3429 cm^{-1} (–OH), 1623 cm^{-1} (C=C) [36], and 1165 cm^{-1} (C–H) [37], and the characteristic peaks of functional groups on PS can be clearly seen at 2360 cm^{-1} , 1064 cm^{-1} , and 575 cm^{-1} , which correspond to the cumulated double bond (O=S=O), S=O, and ionic bond of potassium, respectively [38–40]. Moreover, a new peak at 860 cm^{-1} corresponds to S–O–C [41]. The appearance of S–O–C verifies that AC and PS are successfully bonded under mechanical action, indicating these two materials have been closely combined to form a stable composite material during the milling process. The broad band at 3429 cm^{-1} corresponds to the stretching vibration of –OH [42,43]. This peak in MAC and M(AC-PS) is slightly stronger than that in AC, and almost disappears in M(AC-PS)-after reaction. The

results showed that $-OH$ is consumed as an active functional group during TC degradation. The other functional groups of M(AC-PS)-after reaction are basically consistent with AC, indicating that the PS bound to the AC is consumed during the reaction.

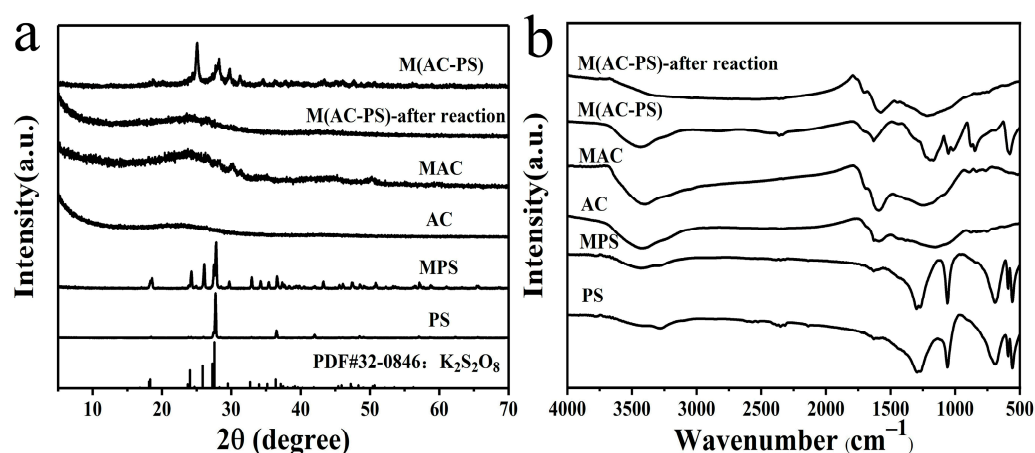


Figure 3. (a) XRD patterns and (b) FT-IR spectra of different materials.

The XPS was employed to detect the surface components of materials, and the obtained spectra of MAC and M(AC-PS) are shown in Figure 4a–f. The total spectrum (Figure S3) shows that MAC has a carbon content of 84.72% (atomic percentage) and an oxygen content of 15.73%. In contrast, M(AC-PS) has a reduced carbon content of 44.34% and an increased oxygen content of 40.81%. At the same time, the sulfur content in M(AC-PS) is 14.85%, and the O/S mass ratio is 2.75, which is much higher than the ratio in PS, indicating the presence of a large number of oxygen-containing functional groups on the AC in M(AC-PS). The C 1s XPS spectrum of MAC (Figure 4a) was deconvoluted into five peaks at 284.8, 286.3, 287.7, 289.3, and 290.4 eV, corresponding to C-C (75.83%) [44], C-OH (16.56%), C=O (carbonyl, 3.11%), O=C-OH (carboxyl, 4.17%), and $\pi-\pi^*$ shake-up satellite (0.36%) [45], respectively. The C1s XPS spectrum of M(AC-PS) (Figure 4b) has six peaks at 284.8, 286.2, 289.8, 290.1, 292.5, and 293 eV, among which 284.8 and 286.2 eV correspond to C-C (14.8%) and C-OH (6.01%), respectively. Both 289.8 and 290.1 eV correspond to O=C-OH (a total of 39.67%), and 292.5 and 293.0 eV correspond to $\pi-\pi^*$ oscillating satellite peaks (a total of 26.15%) [45,46]. The significant increase in $\pi-\pi^*$ satellite in M(AC-PS) indicates the greatly enhanced electron transfer capability of the composite material. The C1s XPS spectrum peaks of M(AC-PS)-after reaction (Figure 4c) are at 284.8, 286.3, 288.5, and 292.0, corresponding to C-C (63.39%), C-OH (17.73%), O=C-OH (13.91%), and $\pi-\pi^*$ (4.97%), respectively. Through the comparative analysis, it was found that from MAC to M(AC-PS) and then to M(AC-PS)-after reaction, the C-OH content first decreased from 16.53% to 6.01% and then increased to 17.73%, and the content of O=C-OH increased from 4.17% to 52.77% and finally decreased to 13.91%. Meanwhile, the $\pi-\pi^*$ oscillating satellite content also decreased to 4.97% after the reaction. These results show that C-OH and some C-C on the AC transform into O=C-OH when the PS is added into the ball milling system, and the generated O=C-OH and $\pi-\pi^*$ oscillating satellites are consumed during the reaction. The O1s XPS spectra (Figure 4d–f) of the above three materials also confirm that the C-OH peak at 532.3 eV significantly decreases after co-ball milling and then increases after the reaction, while the content of C=O at 531.3 eV changes in the opposite way [46]. The two peaks in the S 2p spectrum of M(AC-PS) at 168.5 and 169.8 eV (Figure S4) are attributed to C-SO_x-C and SO₄²⁻, respectively, further proving the bonding of S on the AC [31,47].

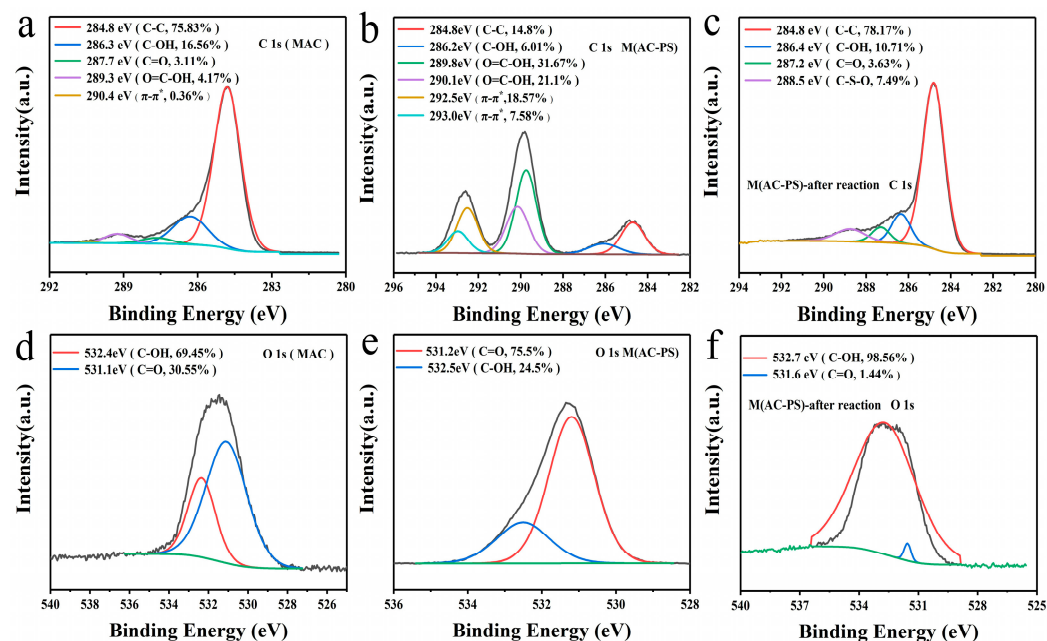


Figure 4. C 1s XPS spectra (a–c) and O 1s XPS spectra (d–f) of MAC, M(AC-PS), and M(AC-PS)-after reaction.

3.2. Catalytic Degradation of TC by M(AC-PS)

3.2.1. Activation and Catalytic Performance of M(AC-PS)

The results of the TC degradation experiments using different materials are shown in Figure 5a and Figure S5. The removal rate of TC (20 mg/L) by AC at a concentration of 0.1 g/L reaches 39.4% in 40 min. Under the same conditions, MAC has a TC removal efficiency of only 24.4%. It can be seen that the ball milling process reduces the adsorption capacity of AC; this result is consistent with the BET analysis results mentioned earlier. The TC removal rate in the PS system is only 3.3%, while it reaches 25.2% in the MPS system, suggesting that the ball milling process has activated the PS. This may also be related to the more exposed crystal planes of the PS after ball milling. In the mixed system of AC and PS (AC/PS), the removal efficiency of TC is 41.9%, almost equal to the sum of the independent removal efficiencies (42.7%) in the AC and PS systems. The removal efficiency of TC by MAC/MPS is 53.1%, slightly higher than the sum of the individual removal efficiencies of MAC and MPS (49.6%). This indicates that AC has almost no activation ability for PS, while MAC has weak activation ability for MPS.

It is noteworthy that the activation ability of AC for PS is greatly enhanced after mixed ball milling. The composite material M(AC-PS) obtained by co-ball milling AC and PS exhibits a removal efficiency of up to 97.3% for TC. Considering the low adsorption performance (24.4%) of MAC, it can be concluded that the removal of TC by M(AC-PS) is mainly due to the oxidative degradation of activated MPS. Combined with the changes in the preferentially exposed crystal planes shown in the above XRD analysis, AC is perhaps more likely to activate PS through the connected (1–11) crystal plane. The pseudo-first-order kinetics can well fit the reaction process of M(AC-PS), also indicating that the removal of TC is not only due to adsorption, but also involves degradation. According to the first-order kinetic fitting analysis (Figure 5b,c), the reaction rate constant of M(AC-PS) is 1.9252 min^{-1} , while the rate constants of PS, MPS, AC, and MAC are 0.05168, 0.06695, 0.08718, and 0.1089 min^{-1} , respectively. It is obvious that the reactivity of M(AC-PS) is much higher. The AC in M(AC-PS) exhibits excellent activation performance in relation to the PS on it. The ball milled composite can be directly used as catalytic oxidation material for TC degradation.

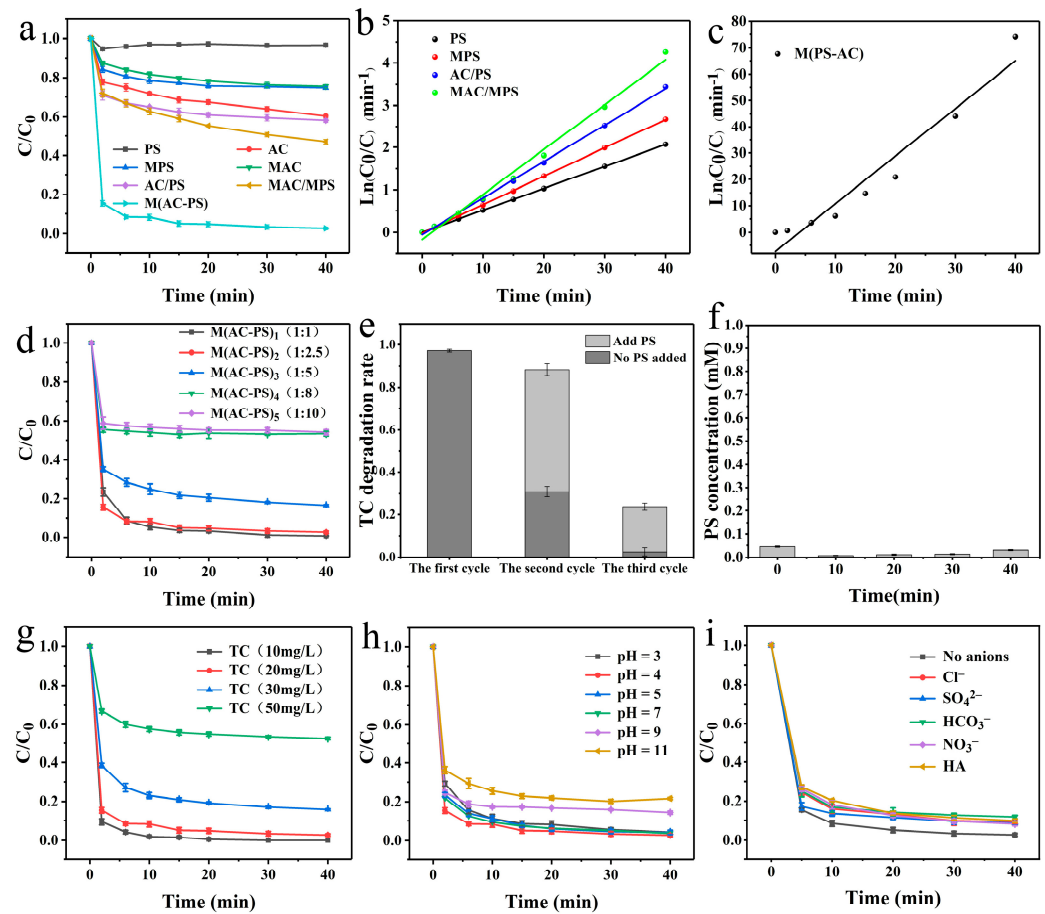


Figure 5. Degradation of TC by various materials (a), the reaction kinetics of PS, MPS, AC/PS, and MAC/MPS system (b), M(AC-PS) system (c), degradation of TC in M(AC-PS) systems with different ratios of AC and PS (d), reusability of M(AC-PS) in TC degradation (e), change in PS concentration in solution (f), the influence of TC concentration (g), pH (h), and inorganic anion and HA (i) on TC removal. Conditions: initial pH of 4, temperature of 25 °C, TC concentration of 20 mg/L, AC/MAC dosage of 0.1 g/L, PS/MPS concentration of 1 mM, M(AC-PS) dosage of 38 mg, and a stirring speed of 220 rpm.

When the mass ratio of AC to PS is 1:1, 1:2.5, 1:5, 1:8, and 1:10, the prepared composite materials achieve TC degradation efficiencies of 99.3%, 97.3%, 83.6%, 46.6%, and 45.8%, respectively (Figure 5d). It can be observed that the degradation efficiency of TC decreases as the mass ratio of AC to PS in M(AC-PS) changes from 1:1 to 1:10. This is because the adsorption capacity of M(AC-PS) significantly decreased with the increase in the PS dosage, and the surface of the AC can only accommodate a certain amount of PS. Excessive PS exists as MPS in the reaction system, resulting in a weaker degradation effect. Considering the cost and efficiency, the optimal mass ratio of AC and PS used in M(AC-PS) is determined to be 1:2.5, and this ratio is applied for subsequent experiments and analysis.

3.2.2. Reusability of M(AC-PS)

To investigate the activation and catalytic stability of solid composite materials, the TC concentration in the M(AC-PS) system was adjusted back to 20 mg/L after the first round of reactions. The reaction systems were then divided into two groups (Figure 5e): the first directly underwent the subsequent reactions, while 1 mM of PS was added to the second group, then the two systems were placed back in the shaker for the next cycle of reactions. After 40 min, the above steps were repeated for the third round of reactions. In the second run, the removal rate of TC in the first group decreased to 30.9%, indicating the PS in the M(AC-PS) was not completely consumed during the first reaction process;

AC in M(AC-PS) can still activate PS to degrade TC. With the consumption of PS and the loss of AC adsorption capacity during the degradation process, the removal rate of TC was only 2.5% in the third run. For the second group with PS addition, the TC degradation rate in the second run reached around 88.3% with the existence of sufficient oxidant, which was significantly higher than the degradation rate (41.9%) of the PS/AC system. This further confirms that the degradation of TC is initiated by the activation of PS by AC, and the ability of the AC in M(AC-PS) to directly activate the connected PS is stronger than its ability to activate the PS in the solution. The interaction between solids significantly improves the activation performance of AC on PS. The TC removal efficiency in the third round decreased to 30.5% due to the rapid loss of surface-active sites on the AC.

Additionally, the PS concentration in the solution during the reaction was measured without adding pollutants to investigate the existing form of PS in the M(AC-PS) reaction system (Figure 5f). It was observed that the PS concentrations were initially only 0.045 mM, and then 0.008, 0.012, 0.014, and 0.031 mM at 10, 20, 30, and 40 min, respectively. According to the proportion of PS in the M(AC-PS), the amount of PS added to the reaction system is 1 mM, which means that the highest amount of PS released into the solution is only 4.5% of the total amount. A large amount of PS exists on the AC and is triggered during the TC degradation process without entering the liquid phase. The small amount of PS present in the solution can also be activated and decomposed by the AC in the M(AC-PS). Furthermore, almost no radicals were detected in the solution of this system, indicating the solid-phase interaction in M(AC-PS) not only improves the activation efficiency of AC on PS, but also significantly enhances the non-radical processes of PS activation.

3.3. Effect of Reaction Conditions on TC Degradation

3.3.1. Effect of TC Concentration

Figure 5g illustrates the removal of TC at different concentrations. Within 20 min, M(AC-PS) can completely remove TC at a concentration of 10 mg/L. When the initial concentrations of TC increase to 20, 30, and 50 mg/L, the removal rates of TC within 40 min reach 97.3%, 84.1%, and 47.5%, respectively. TC needs to be adsorbed onto the surface of AC and then react with the activation product of PS to achieve degradation. At high TC concentrations (>20 mg/L), the adsorption sites and fixed PS on the AC are insufficient, limiting the adsorption and reaction between M(AC-PS) and TC and leading to the decrease in removal efficiency. Compared with the PS-based TC oxidation degradation processes reported in the literatures (Table 2), the solid composite material prepared in this study achieves good removal efficiency at a lower dosage of AC and PS. Unless otherwise stated, the TC dosage used in subsequent experiments is 20 mg/L.

Table 2. Comparison of parameters in different research.

| Activator | Preparation Method | TC Dosage | Activator Dosage | PS Dosage | Degradation Rate | Reaction Time |
|-----------|--------------------------|-----------|------------------|-----------|------------------|-------------------|
| FeS@BC | Physical ball milling | 200 mg/L | 0.05 g/L | 10 mM | 87% | 30 min [19] |
| BCM50 | Physical ball milling | 20 mg/L | 0.02 g/L | 0.5 mM | 69.30% | 60 min [48] |
| Fe-N@MFC | Chemical process | 5 mg/L | 0.5 g/L | 1.8 mM | 90.50% | 60 min [49] |
| MRSB | Chemical process | 20 mg/L | 1 g/L | 8 mM | 87.05% | 120 min [2] |
| Co-CN | Chemical process | 10 mg/L | 0.5 g/L | 0.8 mM | 99.30% | 24 min [50] |
| AC | Physical co-ball milling | 20 mg/L | 0.1 g/L | 1 mM | 97.3% | 40 min This study |

3.3.2. Effect of pH

For reaction systems utilizing carbon materials to activate PS, pH is a key factor affecting the AOPs reactions, and its impact is significant. Therefore, the influences of initial pH on TC degradation in the M(AC-PS) system were investigated. This is shown in

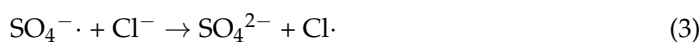
Figure 5h. When the pH value is below 7, TC can be quickly removed, with a degradation rate of over 95% within 40 min. At pH 4, the first-order kinetic constant of reaction reaches the maximum of 1.9525 min^{-1} . When the pH is above 7, the degradation rate of TC begins to decrease. At pH 9, the degradation rate is 85.7%, and it further decreases to 78.4% at pH 11.

It is clear that M(AC-PS) exhibits higher degradation performance under neutral and acidic conditions, where AC has better activation ability for PS. The changes in TC degradation with pH may be attributed to the following factors. On the one hand, the pH change affects the charge distribution on the carbon material surface. In low pH environments, the concentration of surface hydrogen ions on M(AC-PS) increases, enhancing the activity of acidic functional groups (e.g., $\text{O}=\text{C}-\text{OH}$). This may make carbon materials more effective in activating PS and enhance their ability to remove TC. On the other hand, the decomposition of PS is hindered under alkaline conditions, resulting in a reduction in $\text{SO}_4^{\cdot-}$ production. $\text{SO}_4^{\cdot-}$ can react with hydroxide ions to generate $\cdot\text{OH}$, as shown in Equation (1) [51]. Furthermore, $\cdot\text{OH}$ can further react with OH^- to generate water (Equation (2)), leading to the elimination of radicals.



3.3.3. Effect of Inorganic Anions and Natural Organic Matter

In natural water bodies, there are often multiple co-existing inorganic anions that can potentially influence the pollutant degradation process. Therefore, the effects of common inorganic anions such as NO_3^- , Cl^- , HCO_3^- , and SO_4^{2-} on TC degradation were investigated (Figure 5i). With the addition of Cl^- , NO_3^- , HCO_3^- , and SO_4^{2-} , the TC degradation rate decreased from 97.3% to 90.8%, 91.5%, 88.2%, and 91.9%, respectively. This indicates a slight negative effect of Cl^- on TC degradation. The reason is that Cl^- can react with $\text{SO}_4^{\cdot-}$ and $\cdot\text{OH}$ to produce other low oxidation state species as shown in Equations (3)–(7) [2], leading to a decrease in the TC degradation rate. Compared to other anions, NO_3^- and SO_4^{2-} have a smaller impact on the degradation rate of TC, which may be due to their ability to generate species with slightly lower oxidation–reduction potentials and slower reaction rates when reacting with $\text{SO}_4^{\cdot-}$ and $\cdot\text{HO}$ [52]. HCO_3^- can react with $\cdot\text{HO}$ and $\text{SO}_4^{\cdot-}$ to generate $\text{HCO}_3\cdot$ with a lower oxidation potential, slowing down the reaction rate, as shown in Equations (8) and (9) [53]. Additionally, the pH increase caused by HCO_3^- hydrolysis can also lead to a decrease in the TC degradation rate. After adding typical natural organic matter humic acid (HA), which is widely present in natural water bodies, the degradation rate of TC decreased to 90.3%. This may be due to the competition between HA and TC for the active species in the solution. Furthermore, HA has strong π - π stacking, which is easily adsorbed on the catalyst surface and covers the active sites [54,55]. In general, M(AC-PS) maintains a high TC degradation rate in the presence of inorganic ions and HA.



3.4. Possible Mechanism of TC Degradation by M(AC-PS)

3.4.1. Identification of Reactive Oxygen Species in Reactions

Free radical scavenging experiments were carried out in the MPS/TC and M(AC-PS)/TC degradation systems to identify the active substances produced by PS activation (Figure 6a,b). Methanol (MeOH), tert-butanol (TBA), and L-histidine (L-His) were used to quench $\cdot\text{HO}$ and $\text{SO}_4^{\cdot-}$, $\cdot\text{HO}$, and $^1\text{O}_2$, respectively [56,57]. The degradation of TC by MPS decreased from 25.2% to 8.3% with the addition of MeOH or TBA. This inhibition suggests that the oxidation of TC by MPS is mainly attributed to $\cdot\text{HO}$, and the ball milling process can activate PS to produce $\cdot\text{HO}$. For the M(AC-PS) system, the degradation rate of TC decreased from 97.3% to 91.3%, 71.8%, and 63.3% after the addition of MeOH, TBA, and L-His, respectively, suggesting that a small amount of $\cdot\text{HO}$ and $\text{SO}_4^{\cdot-}$ participated in the reaction. Due to the limitation of solid–liquid interface conduction [58] after the MPS is fixed on the MAC, the quencher in the solution cannot capture the reactive oxygen species (ROS) generated on the MAC surface in time, leading to the inhibition effect of adding MeOH on TC degradation was lower than that of adding TBA. According to the result of the L-His scavenging experiment, $^1\text{O}_2$ is involved in this reaction process, indicating that TC oxidation in the M(AC-PS) system mainly occurs through the non-radical mechanism.

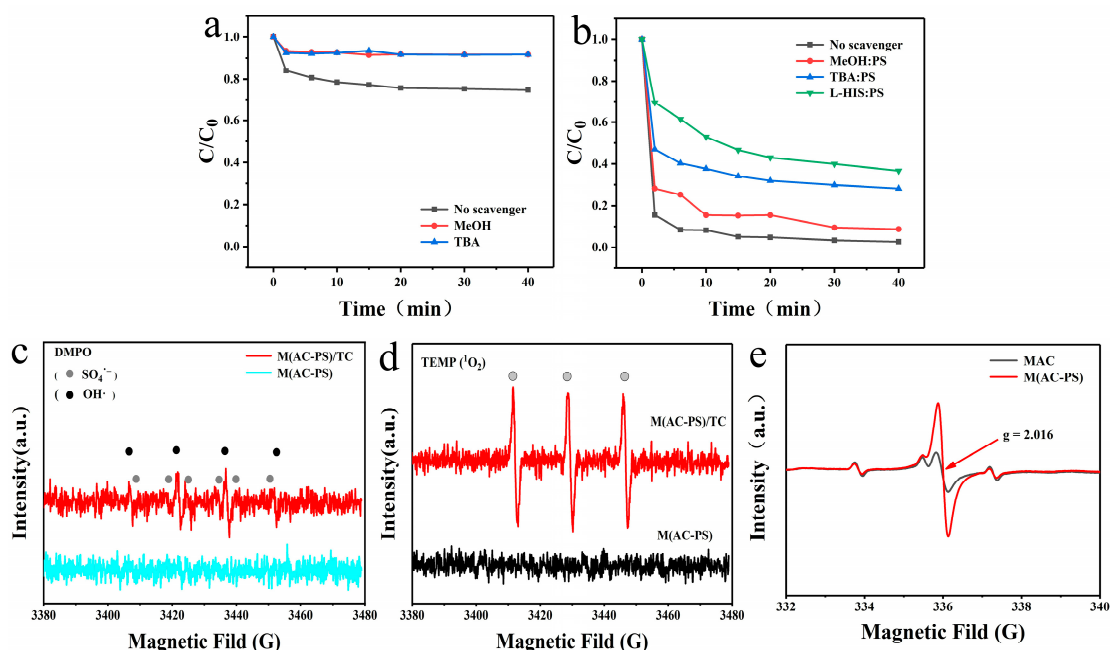


Figure 6. Effect of free radical quencher on TC degradation by (a) MPS and (b) M(AC-PS). Conditions: pH = 4, T = 25 °C, M(AC-PS) dose = 38 mg, and TC concentration = 20 mg/L. EPR spectra of (c) hydroxyl and sulfate radicals, (d) singlet oxygen, and (e) electron hole in different systems.

In order to further determine the produced ROS and reaction mechanism of the M(AC-PS) system, an EPR test was performed using 5,5-dimethyl-1-pyrrolidinium n-oxide (DMPO) and 2,2,6,6-tetramethyl-4-piperidinol (TEMP) as spin trapping agents. As shown in Figure 6c, weak DMPO($\cdot\text{HO}$) and DMPO($\text{SO}_4^{\cdot-}$) signals were observed in the M(AC-PS)/TC system, indicating that a small amount of MPS is activated by MAC to produce free radicals, which is consistent with the results of the scavenging experiments. These results indicate that free radicals are not the main active substances causing TC degradation in the M(AC-PS) system. As shown in Figure 6d, high intensity $^1\text{O}_2$ characteristic peaks were observed in the M(AC-PS)/TC system, which are not present in the M(AC-PS) system. It can be observed that the non-free radical effect of single-linear oxygen begins to appear after the addition of TC. However, there is still a TC removal rate of 63.3% in the scavenging experiment with the addition of L-His, as shown in Figure 6b, indicating that there are other degradation mechanisms in the M(AC-PS)/TC system. Ghosh et al. reported that

the catalytic degradation of organic pollutants by carbon materials can also be achieved through the electron transfer mechanism [59]. In Figure 6e, it is found that unlike the MAC system, electron holes [60] with a g value of 2.016 exist in the M(AC-PS) system [61]. This may be due to the active electron migration in the π -bond of AC during the ball milling process [62], which may provide an electron transfer pathway in the reaction. The above XPS analysis also demonstrated a significant increase in π - π^* in the M(AC-PS).

3.4.2. Analysis of the TC Degradation Mechanism of M(AC-PS)

The free radical scavenging experiment and EPR testing results reveal that $^1\text{O}_2$ is the main active species involved in the oxidative degradation of TC. It was reported that C=O can form an epoxy structure under the action of PS, which can activate another PS molecule to generate $^1\text{O}_2$, thereby oxidizing and degrading organic pollutants [63,64]. In XPS analysis, more C=O bonds were also found on the M(AC-PS). Furthermore, the $^1\text{O}_2$ scavenging experiment exhibits the existence of other reaction mechanisms in TC degradation. XPS and EPR analyses demonstrate the significant increase in π - π^* and electron holes in the M(AC-PS), which potentially facilitate an electron transfer process. According to reports, PS can be electrostatically adsorbed onto carbon materials through π -bonds and sp^2 hybridized electrons, and then transfer electrons through electron holes on AC [65,66]. In this study, a complex is formed between PS and AC, and electrons may be directly taken from TC in the oxidation reaction.

Apart from the $^1\text{O}_2$, the electron transfer pathway is also important for achieving highly selective degradation of pollutants in AOPs technology. To further determine the degradation mechanism of TC by M(AC-PS), the electron transfer process was verified by electrochemical tests (Figure 7). When the prepared material was used as an electrode, the internal electron transfer ability of the material and the electron transport between material and contaminant can be confirmed by the current changes in the presence or absence of PS and before and after the addition of TC [67,68]. From the i - t curves of MAC and M(AC-PS) (Figure 7a), it can be observed that the current in the M(AC-PS) system gradually decreases to a stable value, while the current in the MAC system remains at 0 in the three-electrode system, indicating the better conductivity of M(AC-PS). After the addition of TC, the currents in both the M(AC-PS) and MAC systems fluctuate, and finally stabilize again, which shows that TC provides electrons as an electron donor in the process of TC degradation, resulting in a weak current. There is direct electron transfer between M(AC-PS) and TC. According to the CV curve (Figure 7b), M(AC-PS) has a wider open circuit voltage range compared to MAC, and also shows a better electron conduction ability. Based on the above analysis, it can be concluded that the degradation of TC by M(AC-PS) is mainly a non-free radical process involving singlet oxygen and direct electron transfer mechanisms (Figure 8), rather than being predominantly controlled by the free radical mechanism as reported in most of the literature. This avoids the problem of reactive consumption of free radicals from other substances, and greatly improves the degradation efficiency of TC.

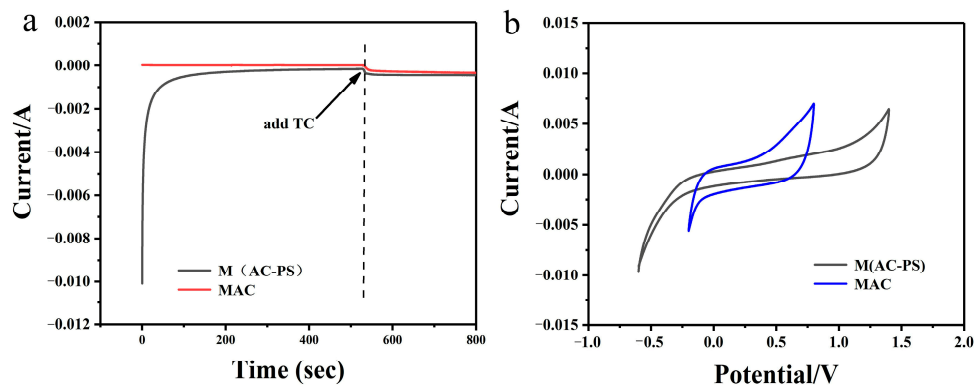


Figure 7. EIS (a) and CV curve (b) of MAC and M(AC-PS).



Figure 8. The proposed mechanism for TC degradation in the M(AC-PS) system.

4. Conclusions

In this study, M(AC-PS) was successfully synthesized using the physical ball milling method and exhibited effective degradation performance on TC. Exploring the effects of reaction conditions on degradation, it was found that the TC removal efficiency is more than 97% under both acidic and neutral conditions when the ratio of AC to PS is 1:2.5. Inorganic anions had a slight inhibitory effect on TC removal, with the following order: $\text{HCO}_3^- > \text{Cl}^- > \text{HA} > \text{SO}_4^{2-} > \text{NO}_3^-$. Mechanistically, the significantly improved TC oxidation degradation performance in the M(AC-PS) system can be attributed to the synergistic effect generated during the ball milling process. An effective connection is formed between AC and PS. The AC, after co-milling, can provide activation sites for PS and serve as a medium for electron conduction. The PS bound onto the AC can not only be activated by the surface functional groups to generate $^1\text{O}_2$, but can also directly interact with TC through the rapid electron transfer function of AC. Additionally, the activation process is mainly carried out in a solid composite catalyst, with only a trace amount of PS being dissolved in the solution, providing a more convenient and effective way to utilize the catalyst. Therefore, M(AC-PS) appears to be a promising green material for the in situ remediation of contaminated water bodies.

Supplementary Materials: The following supporting information can be downloaded at: <https://www.mdpi.com/article/10.3390/pr12040672/s1>, Figure S1: TEM images of (a) AC and (b) M(AC-PS), Figure S2: EDS spectrum of M(AC-PS), Figure S3: XPS total spectrum of MAC and M(AC-PS), Figure S4: XPS S 2p spectrum of M(AC-PS).

Author Contributions: Conceptualization, P.T. and Y.H.; methodology, P.T. and X.C.; formal analysis, P.T. and X.Z.; investigation, N.M. and X.C.; resources, X.Z. and Y.H.; data curation, N.M.; writing—original draft preparation, P.T.; writing—review and editing, W.W. and T.L.; supervision, W.W. and T.L.; project administration, W.W.; funding acquisition, W.W. All authors have read and agreed to the published version of the manuscript.

Funding: This research was funded by the Tianjin Key Research and Development Plan of China (22YFYZHZ003000), the National Natural Science Foundation of China (No. 22376107, 22176102, 22036004 and 42277056), the Joint Funds of the National Natural Science Foundation of China (No. U23B20165), and the NCC Fund of China.

Data Availability Statement: Data are contained within the article and Supplementary Materials.

Conflicts of Interest: The authors declare that the research was conducted in the absence of any commercial or financial relationships that could be construed as a potential conflict of interest.

References

1. Dai, Y.; Liu, M.; Li, J.; Yang, S.; Sun, Y.; Sun, Q.; Wang, W.; Lu, L.; Zhang, K.; Xu, J.; et al. A review on pollution situation and treatment methods of tetracycline in groundwater. *Sep. Sci. Technol.* **2020**, *55*, 1005–1021. [CrossRef]
2. Huang, H.; Guo, T.; Wang, K.; Li, Y.; Zhang, G. Efficient activation of persulfate by a magnetic recyclable rape straw biochar catalyst for the degradation of tetracycline hydrochloride in water. *Sci Total Environ.* **2021**, *758*, 143957. [CrossRef] [PubMed]

3. Annamalai, S.; Shin, W.S. Efficient degradation of trimethoprim with ball-milled nitrogen-doped biochar catalyst via persulfate activation. *Chem. Eng. J.* **2022**, *440*, 135815. [[CrossRef](#)]
4. Hu, X.; Jia, L.; Cheng, J.; Sun, Z. Magnetic ordered mesoporous carbon materials for adsorption of minocycline from aqueous solution: Preparation, characterization and adsorption mechanism. *J. Hazard. Mater.* **2019**, *362*, 1–8. [[CrossRef](#)] [[PubMed](#)]
5. Li, Z.; Guo, C.; Lyu, J.; Hu, Z.; Ge, M. Tetracycline degradation by persulfate activated with magnetic Cu/CuFe₂O₄ composite: Efficiency, stability, mechanism and degradation pathway. *J. Hazard. Mater.* **2019**, *373*, 85–96. [[CrossRef](#)] [[PubMed](#)]
6. Li, C.; Yu, S.; Che, H.; Zhang, X.; Han, J.; Mao, Y.; Wang, Y.; Liu, C.; Dong, H.J. Fabrication of Z-Scheme heterojunction by anchoring mesoporous gamma-Fe₂O₃ Nanospheres on g-C₃N₄ for degrading tetracycline hydrochloride in water. *ACS Sustain. Chem. Eng.* **2018**, *6*, 16437. [[CrossRef](#)]
7. Yu, J.; Kiwi, J.; Zivkovic, I.; Ronnow, H.M.; Wang, T.; Rtimi, S. Quantification of the local magnetized nanotube domains accelerating the photocatalytic removal of the emerging pollutant tetracycline. *Appl. Catal. B Environ.* **2019**, *248*, 450. [[CrossRef](#)]
8. Wei, J.; Liu, Y.; Zhu, Y.; Li, J. Enhanced catalytic degradation of tetracycline antibiotic by persulfate activated with modified sludge bio-hydrochar. *Chemosphere* **2020**, *247*, 125854. [[CrossRef](#)] [[PubMed](#)]
9. Hegde, V.; Uthappa, U.T.; Mane, P.; Ji, S.M.; Suneetha, M.; Wang, B.; Altalhi, T.; Subrahmanya, T.M.; Kurkuri, M.D. Design of low-cost natural casein biopolymer based adsorbent for efficient adsorption of multiple anionic dyes and diclofenac sodium from aqueous solutions. *Chemosphere* **2024**, *353*, 141571. [[CrossRef](#)] [[PubMed](#)]
10. Miao, L.; Chen, F.; Zhang, Z.; Li, D.; Hassan, M.; Gong, Z.; Feng, Y. Insights on enhanced antibiotic sulfamethoxazole removal by magnetic activated carbon-ballasted coagulation: Efficacy and floc properties. *Sep. Sci. Technol.* **2023**, *315*, 123643.
11. Li, D.; Zhan, W.; Gao, X.; Wang, Q.; Li, L.; Zhang, J.; Cai, G.; Zuo, W.; Tian, Y. Aminated waste paper membrane for efficient and rapid filtration of anionic dyes and antibiotics from water. *Chem. Eng. J.* **2023**, *455*, 140641. [[CrossRef](#)]
12. Wang, D.; Xin, S.; Dong, Y.; Sun, Z.; Li, X.; Wang, Q.; Liu, G.; Liu, Y.; Xin, Y. Heat and carbon co-activated persulfate to regenerate gentamicin-laden activated carbon: Performance, mechanism, and safety assessment. *Chemosphere* **2024**, *349*, 140960. [[CrossRef](#)] [[PubMed](#)]
13. Kumar, S.; Tewari, C.; Sahoo, N.G.; Philip, L. Mechanistic insights into carbo-catalyzed persulfate treatment for simultaneous degradation of cationic and anionic dye in multicomponent mixture using plastic waste-derived carbon. *J. Hazard. Mater.* **2022**, *435*, 128956. [[CrossRef](#)] [[PubMed](#)]
14. Tian, K.; Hu, L.; Li, L.; Zheng, Q.; Xin, Y.; Zhang, G. Recent advances in persulfate-based advanced oxidation processes for organic wastewater treatment. *Chin. Chem. Lett.* **2022**, *33*, 4461–4477. [[CrossRef](#)]
15. Wang, B.; Wang, Y. A comprehensive review on persulfate activation treatment of wastewater. *Sci. Total Environ.* **2022**, *831*, 154906. [[CrossRef](#)] [[PubMed](#)]
16. Gao, Y.; Wang, Q.; Ji, G.; Li, A. Degradation of antibiotic pollutants by persulfate activated with various carbon materials. *Chem. Eng. J.* **2022**, *429*, 132387. [[CrossRef](#)]
17. Lee, D.; Kim, S.; Tang, K.; Volder, M.D.; Hwang, Y. Oxidative degradation of tetracycline by magnetite and persulfate: Performance, water matrix effect, and reaction mechanism. *Nanomaterials* **2021**, *11*, 2292. [[CrossRef](#)] [[PubMed](#)]
18. Ike, I.A.; Linden, K.G.; Orbell, J.D.; Duke, M. Critical review of the science and sustainability of persulphate advanced oxidation processes. *Chem. Eng. J.* **2018**, *338*, 651–669. [[CrossRef](#)]
19. He, J.; Tang, J.; Zhang, Z.; Wang, L.; Liu, Q.; Liu, X. Magnetic ball-milled FeS@biochar as persulfate activator for degradation of tetracycline. *Chem. Eng. J.* **2021**, *404*, 126997. [[CrossRef](#)]
20. Guan, C.; Jiang, J.; Pang, S.; Ma, J.; Chen, X.; Lim, T. Nonradical transformation of sulfamethoxazole by carbon nanotube activated peroxydisulfate: Kinetics, mechanism and product toxicity. *Chem. Eng. J.* **2019**, *378*, 122147. [[CrossRef](#)]
21. Oh, W.D.; Lua, S.K.; Dong, Z.; Lim, T.T. Performance of magnetic activated carbon composite as peroxymonosulfate activator and regenerable adsorbent via sulfate radical-mediated oxidation processes. *J. Hazard. Mater.* **2015**, *284*, 1–9. [[CrossRef](#)]
22. Song, H.; Yan, L.; Jiang, J.; Ma, J.; Pang, S.; Zhai, X.; Zhang, W.; Li, D. Enhanced degradation of antibiotic sulfamethoxazole by electrochemical activation of PDS using carbon anodes. *Chem. Eng. J.* **2018**, *344*, 12–20. [[CrossRef](#)]
23. An, L.; Xiao, P. Zero-valent iron/activated carbon microelectrolysis to activate peroxydisulfate for efficient degradation of chlortetracycline in aqueous solution. *RSC Adv.* **2020**, *10*, 19401–19409. [[CrossRef](#)]
24. Ushani, U.; Lu, X.; Wang, J.; Zhang, Z.; Dai, J.; Tan, Y.; Wang, S.; Li, W.; Niu, C.; Cai, T.; et al. Sulfate radicals-based advanced oxidation technology in various environmental remediation: A state-of-the-art review. *Chem. Eng. J.* **2020**, *402*, 126232. [[CrossRef](#)]
25. Lyu, H.; Gao, B.; He, F.; Zimmerman, A.R.; Ding, C.; Huang, H.; Tang, J. Effects of ball milling on the physicochemical and sorptive properties of biochar: Experimental observations and governing mechanisms. *Environ. Pollut.* **2018**, *233*, 54–63. [[CrossRef](#)]
26. Lyu, H.; Gao, B.; He, F.; Ding, C.; Tang, J.; Crittenden, J.C. Ball-milled carbon nanomaterials for energy and environmental applications. *ACS Sustain. Chem. Eng.* **2017**, *5*, 9568–9585. [[CrossRef](#)]
27. Amusat, S.O.; Kebede, T.G.; Dube, S.; Nindi, M.M. Ball-milling synthesis of biochar and biochar-based nanocomposites and prospects for removal of emerging contaminants: A review. *J. Water Process. Eng.* **2021**, *41*, 101993. [[CrossRef](#)]
28. Gao, J.; Wang, W.; Rondinone, A.J.; He, F.; Liang, L. Degradation of trichloroethene with a novel ball milled Fe-C nanocomposite. *J. Hazard. Mater.* **2015**, *300*, 443–450. [[CrossRef](#)]
29. Hu, Y.; Li, B.; Yu, C.; Fang, H.; Li, Z. Mechanochemical preparation of single atom catalysts for versatile catalytic applications: A perspective review. *Mater. Today* **2023**, *63*, 288–312. [[CrossRef](#)]

30. Liang, C.; Huang, C.; Mohanty, N.; Kurakalva, R.M. A rapid spectrophotometric determination of persulfate anion in ISCO. *Chemosphere* **2008**, *73*, 1540–1543. [[CrossRef](#)]
31. Tian, W.; Zhang, H.; Duan, X.; Sun, H.; Tade, M.O.; Ang, H.M.; Wang, S. Nitrogen- and sulfur-codoped hierarchically porous carbon for adsorptive and oxidative removal of pharmaceutical contaminants. *ACS Appl. Mater. Interfaces* **2016**, *8*, 7184–7193. [[CrossRef](#)] [[PubMed](#)]
32. Niu, L.; Guo, Q.; Xiao, J.; Li, Y.; Deng, X.; Sun, T.; Liu, X.; Xiao, C. The effect of ball milling on the structure, physicochemical and functional properties of insoluble dietary fiber from three grain bran. *Food Res. Int.* **2023**, *163*, 112263. [[CrossRef](#)]
33. Xiao, F.; Pignatello, J.J. Effects of post-pyrolysis air oxidation of biomass chars on adsorption of neutral and ionizable compounds. *Environ. Sci. Technol.* **2016**, *50*, 6276–6283. [[CrossRef](#)]
34. Wang, Y.; Xu, L.; Wei, F.; Ding, T.; Zhang, M.; Zhu, R. Insights into the adsorption mechanism of tetracycline on hierarchically porous carbon and the effect of nanoporous geometry. *Chem. Eng. J.* **2022**, *437*, 135454. [[CrossRef](#)]
35. Yu, Y.; Guo, H.; Zhong, Z.; Wang, A.; Xiang, M.; Xu, S.; Dong, C.; Chang, Z. Fe₃O₄ loaded on ball milling biochar enhanced bisphenol a removal by activating persulfate: Performance and activating mechanism. *J. Environ. Manag.* **2022**, *319*, 115661. [[CrossRef](#)] [[PubMed](#)]
36. Chhabra, V.A.; Deep, A.; Kaur, R.; Kumar, R. Functionalization of graphene using carboxylation process. *IJSETT* **2012**, *4*, 13–19.
37. Marcinauskas, L.; Grigonis, A.; Valinčius, V.; Valatkevičius, P. Surface and structural analysis of carbon coatings produced by plasma jet CVD. *Mater. Sci.* **2007**, *4*, 1320–1392.
38. Caro, J.C.; Lappan, U.; Lunkwitz, K. Insertion of sulfur-containing functional groups into polytetrafluoroethylene (PTFE) by low pressure plasma treatment. *Surf. Coat. Tech.* **1999**, *116–119*, 792–795. [[CrossRef](#)]
39. Țucureanu, V.; Matei, A.; Avram, A.M. FTIR spectroscopy for carbon family study. *Crit. Rev. Anal. Chem.* **2016**, *46*, 502–520. [[CrossRef](#)]
40. Li, H.; Wen, X.; Shao, F.; Zhou, C.; Zhang, Y.; Hu, N.; Wei, H. Interface covalent bonding endowing high-sulfur-loading paper cathode with robustness for energy-dense, compact and foldable lithium-sulfur batteries. *Chem. Eng. J.* **2021**, *412*, 128562. [[CrossRef](#)]
41. Yudianti, R.; Onggo, H.; Sudirman; Saito, Y.; Iwata, T.; Azuma, J.I. Analysis of functional group sited on multi-wall carbon nanotube surface. *Open Mater. Sci. J.* **2011**, *5*, 242–247. [[CrossRef](#)]
42. Zhao, L.; Cao, X.; Mašek, O.; Zimmerman, A. Heterogeneity of biochar properties as a function of feedstock sources and production temperatures. *J. Hazard. Mater.* **2013**, *256–257*, 1–9.
43. Wang, Y.; Liu, Z.; Huang, W.; Lu, J.; Luo, S.; Czech, B.; Li, T.; Wang, H. Capture-reduction mechanism for promoting Cr(VI) removal by sulfidated microscale zerovalent iron/sulfur-doped graphene-like biochar composite. *Carbon Res.* **2023**, *2*, 11. [[CrossRef](#)]
44. Ding, S.; Tan, P.; Wen, J.; Li, T.; Wang, W. Quantification of 2-chlorohydroquinone based on interaction between N-doped carbon quantum dots probe and photolysis products in fluorescence system. *Sci. Total Environ.* **2022**, *814*, 152745. [[CrossRef](#)]
45. Masud, M.A.A.; Shin, W.S.; Kim, D.G. Degradation of phenol by ball-milled activated carbon (ACBM) activated dual oxidant (persulfate/calcium peroxide) system: Effect of preadsorption and sequential injection. *Chemosphere* **2023**, *312*, 137120. [[CrossRef](#)]
46. Peng, L.; Duan, X.; Shang, Y.; Gao, B.; Xu, X. Engineered carbon supported single iron atom sites and iron clusters from Fe-rich enteromorpha for Fenton-like reactions via nonradical pathways. *Appl. Catal. B-Environ.* **2021**, *287*, 119963. [[CrossRef](#)]
47. Guo, Y.; Zeng, Z.; Zhu, Y.; Huang, Z.; Cui, Y.; Yang, J. Catalytic oxidation of aqueous organic contaminants by persulfate activated with sulfur-doped hierarchically porous carbon derived from thiophene. *Appl. Catal. B-Environ.* **2018**, *220*, 635–644. [[CrossRef](#)]
48. Zhang, W.; Yan, L.; Wang, Q.; Li, X.; Guo, Y.; Song, W.; Li, Y. Ball milling boosted the activation of peroxymonosulfate by biochar for tetracycline removal. *J. Environ. Chem. Eng.* **2021**, *9*, 106870. [[CrossRef](#)]
49. Zhuo, S.; Sun, H.; Wang, Z.; Ren, H.; Xing, D.; Ren, N.; Liu, B. A magnetic biochar catalyst with dual active sites of Fe₃C and Fe₄N derived from floc: The activation mechanism for persulfate on degrading organic pollutant. *Chem. Eng. J.* **2023**, *455*, 140702. [[CrossRef](#)]
50. Zhang, X.; Xu, B.; Wang, S.; Li, X.; Wang, C.; Liu, B.; Han, F.; Xu, Y.; Yu, P.; Sun, Y. Tetracycline degradation by peroxymonosulfate activated with CoN_x active sites: Performance and activation mechanism. *Chem. Eng. J.* **2022**, *431*, 133477.
51. Bekris, L.; Frontistis, Z.; Trakakis, G.; Sygellou, L.; Galiotis, C.; Mantzavinos, D. Graphene: A new activator of sodium persulfate for the advanced oxidation of parabens in water. *Water Res.* **2017**, *126*, 111–121. [[CrossRef](#)]
52. Zhong, Q.; Lin, Q.; Huang, R.; Fu, H.; Zhang, X.; Luo, H.; Xiao, R. Oxidative degradation of tetracycline using persulfate activated by N and Cu codoped biochar. *Chem. Eng. J.* **2020**, *380*, 122608. [[CrossRef](#)]
53. Fu, H.; Zhao, P.; Xu, S.; Cheng, G.; Li, Z.; Li, Y.; Li, K.; Ma, S. Fabrication of Fe₃O₄ and graphitized porous biochar composites for activating peroxymonosulfate to degrade p-hydroxybenzoic acid: Insights on the mechanism. *Chem. Eng. J.* **2019**, *375*, 121980. [[CrossRef](#)]
54. Fu, H.; Ma, S.; Zhao, P.; Xu, S.; Zhan, S. Activation of peroxymonosulfate by graphitized hierarchical porous biochar and MnFe₂O₄ magnetic nanoarchitecture for organic pollutants degradation: Structure dependence and mechanism. *Chem. Eng. J.* **2019**, *360*, 157–170. [[CrossRef](#)]
55. Chen, L.; Ding, D.; Liu, C.; Cai, H.; Qu, Y.; Yang, S.; Gao, Y.; Cai, T. Degradation of norfloxacin by CoFe₂O₄-GO composite coupled with peroxymonosulfate: A comparative study and mechanistic consideration. *Chem. Eng. J.* **2018**, *334*, 273–284. [[CrossRef](#)]

56. Gao, L.; Guo, Y.; Zhan, J.; Yu, G.; Wang, Y. Assessment of the validity of the quenching method for evaluating the role of reactive species in pollutant abatement during the persulfate-based process. *Water Res.* **2022**, *221*, 118730. [[CrossRef](#)]
57. Wu, B.; Arnold, W.A.; Ma, L. Photolysis of atrazine: Role of triplet dissolved organic matter and limitations of sensitizers and quenchers. *Water Res.* **2021**, *190*, 116659. [[CrossRef](#)]
58. Tariq, B.; Mansha, A.; Asim, S.; Kausar, A. Effect of substituents on solubility, medicinal, absorption, emission and cationic/anionic detection properties of anthraquinone derivatives. *J. Fluoresc.* **2023**, 1–18. [[CrossRef](#)]
59. Ghosh, I.; Khamrai, J.; Savateev, A.; Shlapakov, N.; Antonietti, M.; König, B. Organic semiconductor photocatalyst can bifunctionalize arenes and heteroarenes. *Science* **2019**, *365*, 360–366. [[CrossRef](#)]
60. Hu, R.; Chu, L.; Zhang, J.; Li, X.; Huang, W. Carbon materials for enhancing charge transport in the advancements of perovskite solar cells. *J. Power Sources* **2017**, *361*, 259–275. [[CrossRef](#)]
61. Zhai, G.; Zhou, J.; Xie, M.; Jia, C.; Hu, Z.; Xiang, H.; Zhu, M. Improved photocatalytic property of lignin-derived carbon nanofibers through catalyst synergy. *Int. J. Biol. Macromol.* **2023**, *233*, 123588. [[CrossRef](#)]
62. Shi, L.; Wang, T.; Zhang, H.; Chang, K.; Ye, J. Electrostatic self-assembly of nanosized carbon nitride nanosheet onto a zirconium metal–organic framework for enhanced photocatalytic CO₂ reduction. *Adv. Funct. Mater.* **2015**, *25*, 5260–5367. [[CrossRef](#)]
63. Cheng, X.; Guo, H.; Zhang, Y.; Wu, X.; Liu, Y. Non-photochemical production of singlet oxygen via activation of persulfate by carbon nanotubes. *Water Res.* **2017**, *113*, 80–88. [[CrossRef](#)] [[PubMed](#)]
64. Zhou, Y.; Jiang, J.; Gao, Y.; Ma, J.; Pang, S.; Li, J.; Lu, X.; Yuan, L. Activation of peroxymonosulfate by benzoquinone: A novel nonradical oxidation process. *Environ. Sci. Technol.* **2015**, *49*, 12941–12950. [[CrossRef](#)] [[PubMed](#)]
65. Ren, W.; Xiong, L.; Nie, G.; Zhang, H.; Duan, X.; Wang, S. Insights into the electron-transfer regime of peroxydisulfate activation on carbon nanotubes: The role of oxygen functional groups. *Environ. Sci. Technol.* **2020**, *54*, 1267–1275. [[CrossRef](#)] [[PubMed](#)]
66. Nie, C.; Dai, Z.; Meng, H.; Duan, X.; Qin, Y.; Zhou, Y.; Ao, Z.; Wang, S.; An, T. Peroxydisulfate activation by positively polarized carbocatalyst for enhanced removal of aqueous organic pollutants. *Water Res.* **2019**, *166*, 115043. [[CrossRef](#)] [[PubMed](#)]
67. Wang, Y.; Qiao, L.; Zhang, X.; Liu, Z.; Li, T.; Wang, H. Green synthesis of FeCu@biochar nanocomposites through a mechanochemical method for enhanced tetracycline degradation via peroxymonosulfate activation. *Sep. Sci. Technol.* **2024**, *328*, 125077. [[CrossRef](#)]
68. Wang, Y.; Liu, Z.; Huang, P.; Lei, B.; Qiao, L.; Li, T.; Lin, K.; Wang, H. Mechanochemical synthesis of biochar encapsulated FeMn nanoparticles with strong metal–carbon interactions for efficient degradation of tetracycline via activating peroxymonosulfate. *Chem. Eng. J.* **2024**, *479*, 147525. [[CrossRef](#)]

Disclaimer/Publisher’s Note: The statements, opinions and data contained in all publications are solely those of the individual author(s) and contributor(s) and not of MDPI and/or the editor(s). MDPI and/or the editor(s) disclaim responsibility for any injury to people or property resulting from any ideas, methods, instructions or products referred to in the content.